Evidence of a first-order smectic-hexatic transition and its proximity to a tricritical point in smectic films

Ivan A. Zaluzhnyy, Ruslan P. Kurta, Nastasia Mukharamova, Young Yong Kim, Ruslan M. Khubbutdinov, Dmitry Dzhigaev, Vladimir V. Lebedev, Elena S. Pikina, Efim I. Kats, Noel A. Clark, Michael Sprung, Boris I. Ostrovskii, and Ivan A. Vartanyants

Phys. Rev. E **98**, 052703 — Published 16 November 2018

DOI: 10.1103/PhysRevE.98.052703

Evidence of a first-order smectic-hexatic transition and its proximity to tricritical point in smectic films

Ivan A. Zaluzhnyy,[1,2] Ruslan P. Kurta,[3] Nastasia Mukharamova,[1] Young Yong Kim,[1] Ruslan M. Khubbutdinov,[1,2,4] Dmitry Dzhigaev,[1] Vladimir V. Lebedev,[5,6] Elena S. Pikina,[5,4,*] Efim I. Kats,[5] Noel A. Clark,[7,8] Michael Sprung,[1] Boris I. Ostrovskii,[9,4,†] and Ivan A. Vartanyants[1,2,‡]

[1] *Deutsches Elektronen-Synchrotron DESY, Notkestraße 85, D-22607 Hamburg, Germany*
[2] *National Research Nuclear University MEPhI (Moscow Engineering Physics Institute), Kashirskoe shosse 31, 115409 Moscow, Russia*
[3] *European XFEL GmbH, Holzkoppel 4, D-22869 Schenefeld, Germany*
[4] *Institute of Solid State Physics, Russian Academy of Sciences, Academician Ossipyan str. 2, 142432 Chernogolovka, Russia*
[5] *Landau Institute for Theoretical Physics, Russian Academy of Sciences, pr. akademika Semenova 1-A, 142432 Chernogolovka, Russia*
[6] *National Research University Higher School of Economics, Myasnitskaya ul. 20, 101000 Moscow, Russia.*
[7] *Department of Physics, University of Colorado Boulder, Boulder, CO 80309, USA*
[8] *Soft Materials Research Center, University of Colorado Boulder, Boulder, CO 80309, USA*
[9] *Federal Scientific Research Center "Crystallography and photonics", Russian Academy of Sciences, Leninskii prospect 59, 119333 Moscow, Russia*

(Dated: October 5, 2018)

Experimental and theoretical studies of a smectic-A – hexatic-B trasition in freely suspended films of thickness 2-10 µm of the 54COOBC compound are presented. X-ray investigations revealed a discontinuous first-order transition into the hexatic phase. The temperature region of two phase coexistence near the phase transition point diminishes with decreasing film thickness. The width of this temperature region as a function of the film thickness was derived on the basis of a Landau mean-field theory in the vicinity of a tricritical point (TCP). Close to TCP the surface hexatic-B order penetrates anomalously deep into the film interior.

INTRODUCTION

Phase transitions are one of the richest and most intriguing phenomena in modern physics [1, 2]. Despite of important progress in the understanding of the origin and fluctuation behavior of various systems the topic still presents many challenging open questions. Among them of special interest are the anomalous behavior and remarkable material properties of the systems in the vicinity of the tricritical point (TCP), where the phase transition changes from second to first order. This includes a study of TCPs in a variety of systems such as liquid crystals (LCs) [3], colloidal crystals [4], and block-copolymers [5–7]. The presence of TCP has been proved and extensively studied in LC mixtures for the nematic to smectic-A (Sm-A) transition [8–10]. A great impact on the development of this field provided recent discovery of fluctuation induced TCPs in skyrmionic magnetic lattices [11–13]. Liquid crystal freely suspended films (FSFs) are particularly suitable to investigate above problems: such films are substrate-free, the alignment of the smectic layers is almost perfect, allowing the study of single-domain samples of various thickness [14, 15]. The FSFs have provided ideal model system for studying the effects of finite size, surface induced ordering, and their influence on the LC phase transitions in vicinity of TCP.

Here we report on the behavior of the first-order Sm-A – hexatic-B (Hex-B) phase transition in LCs and find that it can be tuned close to a TCP by film thickness variation. The Hex-B is a three-dimensional (3D) analogue of the common hexatic phase [16–18]. It can be considered as a stack of parallel molecular layers, in which elongated molecules are oriented on average along the layer normals, exhibiting long-range bond-orientational (BO) order and short-range positional order within each layer [19–21].

Despite three decades of intensive studies, understanding of the Sm-A–Hex-B phase transition is still limited not only in details but even conceptually. According to the Landau theory of phase transitions [3, 22], this transition is characterized by the two-component BO order parameter $\psi = |\psi| \exp(i6\phi)$ (modulus and phase) and therefore the continuous phase transition must follow the universal behavior predicted for such a case. In reality, a number of experiments [15, 21, 23–26] do not support this concept demanding a revision of this simple picture. This has become especially important recently as experiments (x-ray diffraction and calorimetry) grow in resolution and sophistication [25–28].

Here we perform a detailed x-ray study, enabled by a synchrotron-based coherent photon source, of tricritical behavior in the LC forming material 54COOBC (*n*-pentyl-4′-*n*-pentanoyloxy-biphenyl-4-carboxylate) which exhibits a Sm-A–Hex-B phase transition that depends on the effective dimensionality of the sample. In bulk it has the following phase sequence: I (70 °C) Sm-A (55 °C) Hex-B (53 °C) Cr-B [29–32]. A first-order Sm-A–Hex-B

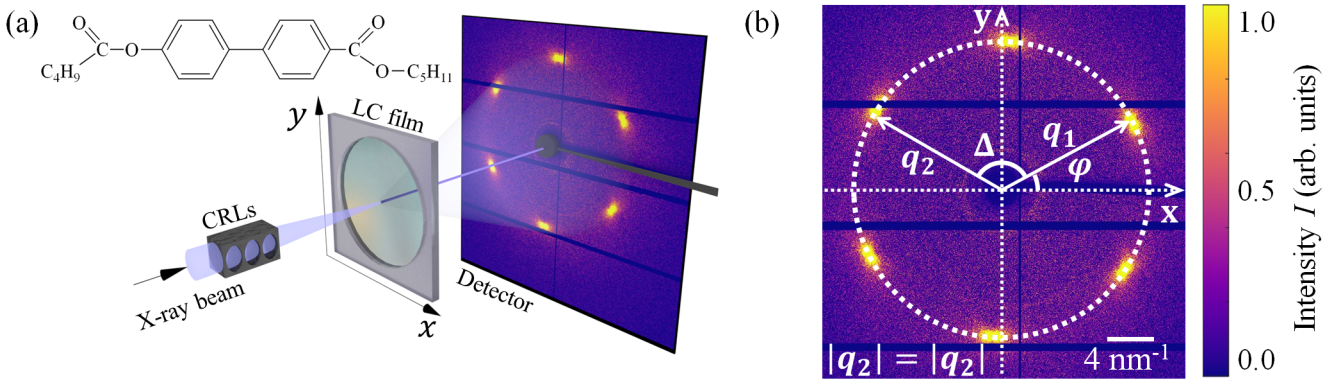

Figure 1. (a) Schematic representation of x-ray diffraction setup used in the experiment. The x-ray beam is focused by CRLs. The free standing LC film is oriented perpendicular to the incoming beam, and piezoelectric motors allow to scan the film in XY-plane. The diffraction pattern is recorder in transmission geometry by Eiger 4M detector placed behind the LC film. The direct beam is blocked by a beamstop. Chemical structure of 54COOBC compound is shown in inset. (b) Example of the diffraction patten from the Hex-B phase and polar coordinate system for evaluation of the angular cross-correlation function $G(q, \Delta)$.

phase transition occurs in bulk samples [23, 29], while very thin FSFs show a continuous Sm-A–Hex-B phase transition [30, 31]. It was argued [31] that this smectic–hexatic phase transition in two-layered 54COOBC films occurs via intermediate Sm-A′ phase, which is characterized by absence of the BO order and increased in-layer positional correlation as compared to the common Sm-A phase. In bulk samples the first-order Sm-A–Hex-B phase transition lies in the vicinity of a TCP. We show that near this TCP the surface ordering penetrates anomalously deep into the interior of the film, which essentially influences the Sm-A–Hex-B phase transition even for thick films, consisting of thousands of layers.

EXPERIMENT

Sample Preparation and Experimental Setup

The freely suspended smectic films of 54COOBC (see for the chemical structure an inset in Fig. 1(a)) were drawn across a circular hole of 2 mm in diameter in a thin glass plate [25, 26, 33]. By varying the temperature and speed of drawing, one can produce films of various thickness, which was measured using AVANTES fiber optical spectrometer. The films were placed inside FS1 sample stage from INSTEC connected to mK1000 temperature controller. The accuracy of temperature control during experiment was about 0.005 °C.

X-ray studies were performed using 13 keV photons (wavelength of 0.954 Å) at the coherence beamline P10 of PETRA III synchrotron source at DESY (Fig. 1(a)). The films were positioned perpendicular to the incident x-ray beam, which was focused by compound refractive lenses (CRLs) to the size of about 2×2 µm^2 at full width at half maximum (FWHM). The scattering signal was recorded by EIGER 4M detector (2070×2167 pixels of 75×75 µm^2 size) placed 232 mm behind the sample. At each temperature the film was scanned with x-ray beam over an area 100×100 µm^2 with a step of 5 µm. Prior to further analysis the collected diffraction patterns were corrected for background scattering and horizontal polarization of synchrotron radiation. Each diffraction pattern was collected at an exposure time of 0.5 s to avoid radiation damage of the film.

Angular X-ray Cross-Correlation Analysis

In this work we used angular x-ray cross-correlation analysis (XCCA) for direct evaluation of the BO order parameters in the Hex-B phase. XCCA is a technique that allows one to study local angular order present in a system by analysis of the angular distribution of the scattered intensity [34–37]. The key element of XCCA is the two-point angular correlation function evaluated for each diffraction pattern [35, 37]

$$G(q_1, q_2, \Delta) = \langle I(q_1, \varphi) I(q_2, \varphi + \Delta) \rangle_\varphi \,. \qquad (1)$$

Here (q, φ) are polar coordinates at the detector plane, Δ is the angular variable, $\langle ... \rangle_\varphi$ denotes averaging over azimuthal angle φ (see Fig. 1(b)). In this work we used the momentum transfer value $q_0 = q_1 = q_2$, where q_0 is a position of the maximum of the scattered intensity. Information about the rotational symmetry of the diffraction pattern is contained in the cross-correlation function defined in Eq. (1) and can be easily analyzed by utilizing angular Fourier components

$$G_n(q) = \frac{1}{2\pi} \int_0^{2\pi} G(q, \Delta) \exp^{-in\Delta} d\Delta \,. \qquad (2)$$

It can be shown [35] that the values of Fourier components $G_n(q)$ are directly related to the angular Fourier components of intensity

$$I_n(q) = \frac{1}{2\pi}\int_0^{2\pi} I(q,\varphi)\exp^{-in\varphi}\,d\varphi \qquad (3)$$

as

$$G_n(q) = |I_n(q)|^2\ . \qquad (4)$$

The angular cross-correlation function $G(q,\Delta)$ as well as its Fourier components $G_n(q)$ can be averaged over an ensemble of diffraction patterns to obtain representative information about the sample and improve signal-to-noise ratio. In contrast, one cannot average individual diffraction patterns or Fourier components of intensity $I_n(q)$, as soon as angular position of the peaks may vary from pattern to pattern [26, 33]. Such averaging may lead to angular smearing of the diffraction peaks, or even produce angular isotropic pattern, that will result in loss of information about the orientational order contained in individual diffraction patterns.

RESULTS

The FSFs of different thickness ranging from 2 µm to 10 µm were measured on cooling and heating to observe formation of the hexatic phase at the Sm-A–Hex-B phase transition. Examples of the measured diffraction patterns in the Sm-A and Hex-B phases are shown in Figs. 2(a)-2(b). The diffraction pattern in the Sm-A phase (Fig. 2(a)) shows typical for liquids broad scattering ring centered at a scattering vector $q_0 \approx 4\pi/a\sqrt{3} \approx 14$ nm^{-1}, where $a \approx 0.5$ nm is the average in-plane intermolecular distance [15, 26]. In the Hex-B phase (Fig. 2(b)) one can readily see sixfold modulation of the in-plane scattering, which is an evidence of the developing BO order.

To describe quantitatively magnitude of the angular modulation of intensity in the Hex-B phase we used the BO order parameters C_{6m} (m is an integer). They are defined as a normalized amplitude of the sixfold angular Fourier components of the azimuthal scattered intensity [20, 25]. The values of C_{6m} can be conveniently determined using the angular XCCA, which allows one to evaluate C_{6m} directly from the measured x-ray diffraction patterns [25, 33, 37]

$$C_{6m} = \left|\frac{I_{6m}(q_0)}{I_0(q_0)}\right| = \sqrt{\frac{G_{6m}(q_0)}{G_0(q_0)}}\ , \qquad (5)$$

where all angular Fourier components are calculated over the ring with the radius q_0. By definition the value of the BO order parameter is normalized, $0 \le C_{6m} \le 1$; in the Sm-A phase $C_{6m} = 0$ for all integer m, while in the Hex-B phase the BO order parameters C_{6m} successively attains non-zero values upon temperature decrease [26, 33, 38]. In this work we analyzed temperature dependence of the fundamental BO order parameter C_6, which is sufficient to distinguish Sm-A and Hex-B phases, while analysis of higher components C_{6m} providing more detailed information of BO order will be a subject of further publication.

Utilizing a microfocused x-ray beam, the spatially resolved maps were retrieved to reveal spatial variation of the BO order parameter C_6 within the scanned area. These maps for 10 μm thick FSF for different temperatures while cooling are shown in Figs. 2(c)-2(f). At high temperature (Fig. 2(c)) the whole FSF is in the Sm-A phase, however, at lower temperatures the film becomes non-uniform. The coexistence of the Sm-A and Hex-B phases can be clearly seen in Figs. 2(d) and 2(e). The Hex-B phase co-exists with the Sm-A phase (Fig. 2(d)) and then, at even lower temperatures, Hex-B becomes dominant and the Sm-A phase exists in the form of regions surrounded by the Hex-B phase (Fig. 2(e)). The size, shape and position of these regions may change when temperature varies, however we always observed the Sm-A phase surrounded by the Hex-B phase in different films of 54COOBC, both on cooling and heating. This observation can be explained by the fact that above the bulk Sm-A–Hex-B phase transition temperature, the hexatic order is first formed at the surface of the film and it penetrates into the inner layers on cooling [15, 23, 39]. For such a mechanism of the Hex-B phase formation, the appearance of the Sm-A regions is favorable, contrary to the nucleation process, for which islands of the Hex-B phase surrounded by the Sm-A phase should be observed. During further cooling the whole FSF turns to the Hex-B phase with formation of single hexatic domains of a lateral size of hundreds of microns (Fig. 2(f)).

In order to perform independent analysis of scattering from the Hex-B and Sm-A regions of the film one needs to find criterion to distinguish between the Sm-A and Hex-B phases. Thus, theoretical criterion $C_6 = 0$ in Sm-A and $C_6 > 0$ in Hex-B does not work for real experimental data due to noise in diffraction patterns, which leads to positive values of C_6 BO order parameter even in the Sm-A phase. To overcome this problem, a statistical analysis of C_6 values was performed, using diffraction patterns measured at different positions of LC film. It turned out, that the the fundamental BO order parameter C_6 in the uniform Sm-A phase (measured at high temperature $T = 59$ °C) has mean value of $\langle C_6\rangle = 0.05$ and standard deviation $\delta C_6 = 0.04$. Based on this analysis, a threshold value $C_t = \langle C_6\rangle + \delta C_6 = 0.09$ was introduced to separate Sm-A and Hex-B phases. Thus, each measured diffraction pattern at any temperature was attributed to one or another phase by following criterion: $C_6 \ge 0.09$ for Hex-B and $C_6 < 0.09$ for Sm-A. This criterion was used throughout the work to perform separate analysis of Sm-A and Hex-B phases.

In Figs. 3(a)-3(d) the temperature dependence of the

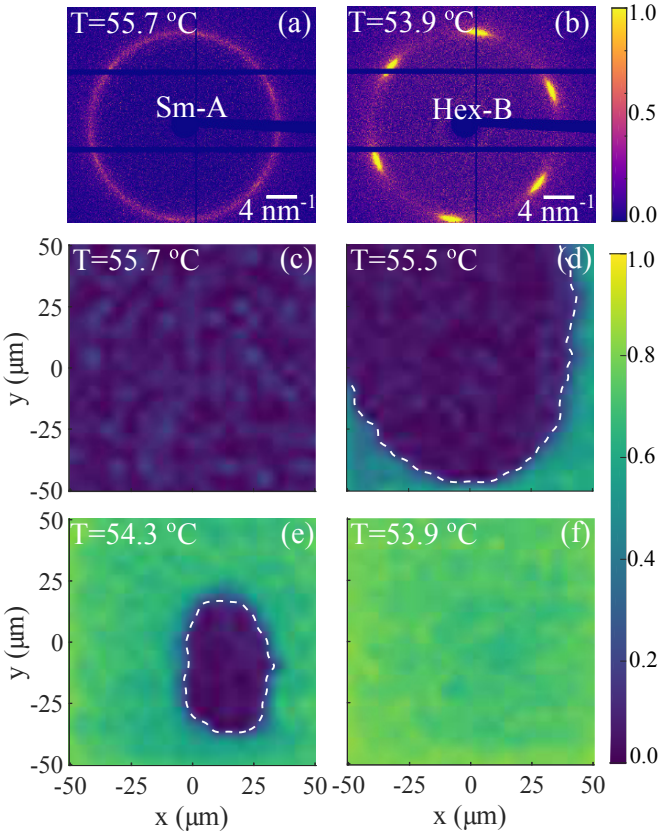

Figure 2. (a-b) Examples of diffraction patterns from 10 μm thick film in the Sm-A (a) and Hex-B (b) phases of 54COOBC. Each image is averaged over 16 diffraction patterns collected within the area of 20×20 μm^2 for better visibility. Color refers to the normalized intensity of the scattered x-rays. (c-d) Spatially resolved maps of BO order parameter C_6 in 100×100 μm^2 region of the 54COOBC film in the Sm-A phase (c), mixed state (d-e) and Hex-B phase (f). Color indicates the local value of C_6, blue (dark) color corresponds to the Sm-A phase, and green (bright) corresponds to Hex-B. Dashed white line marks a border between the Sm-A and Hex-B phases in (d-e).

BO order parameter C_6 for the Sm-A (blue triangles) and Hex-B (red circles) phases for different film thicknesses is shown. This dependence was obtained by averaging the local values of C_6 calculated for each measured diffraction pattern over the regions of Sm-A and Hex-B phases separately (Figs. 2(c)-2(f)). In the Sm-A phase the magnitude of C_6 is vanishingly small and does not change with the temperature. In the Hex-B phase the value of C_6 rises during cooling, which corresponds to an increase of the BO order in the low-temperature hexatic phase. As it is expected for the first-order phase transition the BO order parameter does not change continuously from zero, but instead shows a discontinuous jump of the magnitude of about 0.3 at the temperature where the first areas of the hexatic phase appear in the film. These abrupt changes in values of the BO order parameter unambiguously determine the range of coexistence of the Sm-A and Hex-B phases in both films.

One of the important characteristics of the in-plane short-range order in smectic and hexatic phases is the positional correlation length ξ, determining the length scale over which the positional correlations between the molecules decay [40]. In the Hex-B phase the value of positional correlation length can be calculated as $\xi = 1/\Delta q$, where Δq is a half width at half maximum (HWHM) of the radial cross-section of the hexatic diffraction peak through its maximum. In the Sm-A phase the positional correlation length ξ can be evaluated in a similar way by using the HWHM of the radial cross-section at the smectic scattering ring. In this work we evaluated Δq by fitting the radial intensity profile with Lorentzian function [33, 40].

The temperature dependence of the positional correlation length averaged over regions of the Sm-A and Hex-B phases for different film thicknesses is shown in Figs. 3(e)-3(h). In the Sm-A phase the value of ξ gradually increases from approximately 2.5 nm at the temperature just above the phase transition to about 5 nm at the lowest temperature of the Sm-A phase coexistence. The discontinuity in ξ values at the borders of two phase region is a prime indication of the first-order character of the Sm-A–Hex-B transition in 54COOBC films. In the Hex-B phase the positional correlation length further increases on cooling until the crystal phase is formed. Such a behavior is attributed to coupling between the BO order and positional correlations in the Hex-B phase [33, 41]. Although we did not observed any indications of Sm-A′ phase in thick LC films, qualitatively the growth of the positional correlation length ξ within the two-phase region observed in our experiment resembles the range of enhanced values of the positional correlations reported earlier for a two-layer 54COOBC films [31].

Another important parameter characterizing the Sm-A – Hex-B phase transition is the position of the maximum of scattered intensity q_0 in the smectic and hexatic phases. The value of q_0 is inversely proportional to the average in-plane separation between LC molecules, and thus indicates the variation of density across the transition point. According to the theory of Aeppli and Bruinsma [41] the growing of fluctuations of the BO order parameter in the vicinity of a second-order Sm-A – Hex-B phase transition leads to a continuous increase of the peak's maximum position q_0 and the appearance of inflection point of $q_0(T)$ at phase transition temperature. This is indeed observed for many LC compounds possessing a second-order Sm-A–Hex-B phase transition [26, 33, 42].

Situation becomes different for the first-order Sm-A–Hex-B phase transition, where one can expect a discontinuous density jump at the phase transition point. The discontinuity in q_0 at the borders of the two phase region is readily seen in Figs. 3(i)-3(l), thus providing one more

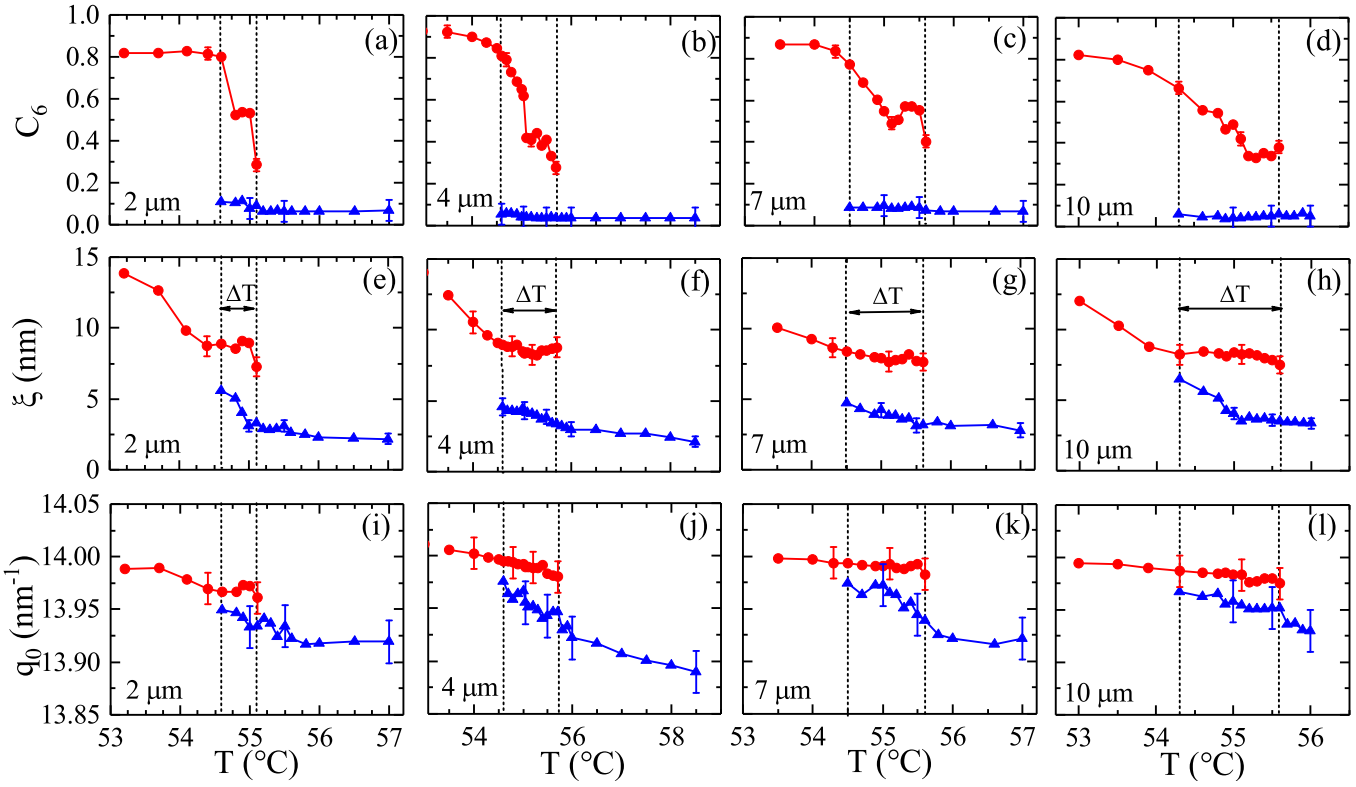

Figure 3. Temperature dependence of the BO order parameter C_6 (a-d), positional correlation length ξ (e-h), and scattering peak maximum position q_0 (i-l) in the Sm-A phase (blue triangles) and Hex-B phase (red circles) close to the region of two phases coexistence. Data are shown for 2 μm (a,e,i), 4 μm (b,f,j), 7 μm (c,g,k), and 10 μm (d,h,l) thick films of 54COOBC. The dashed vertical lines indicate the temperature region ΔT of two phase coexistence. Error bars are shown for every fifth experimental point.

firm evidence for the first-order character of the Sm-A to Hex-B transition in 54COOBC films. The values of q_0 in both coexisting phases differ by about 0.4%, which is rather small for the structural phase transitions of the first order and can be explained by closeness of the system to the TCP.

An important outcome of our experiment was not only the observation of the coexistence of the Sm-A and Hex-B phases over a finite temperature range ΔT but also revealing its dependence on the film thickness (shown by blue circles in Fig. 4). We found that the width of the two-phase coexistence region is about 1.3 K for thick (10 μm) films and decreases for thinner films, reaching the value of about 500 mK for a film with a thickness of 2 μm. These observations are in good agreement with data reported for approximately 0.25 μm thick film (100 molecular layers) of 54COOBC compound, in which coexistence of Sm-A and Hex-B phases was estimated to be within 90 mK [23, 29]. Coexistence of two phases indicates that the average density of the film is intermediate between that of the smectic and hexatic, thereby inducing two-phase equilibrium. Another important observation arising from our experiment is that the value of two-phase region ΔT obtained on cooling is larger than on heating (shown by red triangles in Fig. 4). Such behavior looks natural due to the presence of the hexatic surface ordering in the smectic phase. Thus the Sm-A phase can not be overcooled, but contrary to that the Hex-B phase, can be relatively easy overheated.

THEORY

In the following we derive an analytical expression which models the temperature coexistence width as a function of film thickness. For theoretical analysis of our experimental results let us start with one of the general thermodynamical conditions of the equilibrium coexistence of the Sm-A and Hex-B phases in bulk (apart from the equality of the temperatures)

$$\mu_{\rm H}[T, n_{\rm H}] = \mu_{\rm Sm}[T, n_{\rm Sm}] \ , \qquad (6)$$

where $\mu_{\rm H}[T, n_{\rm H}] = \partial f_{\rm H}[T, n_{\rm H}]/\partial n_{\rm H}$ and $\mu_{\rm Sm}[T, n_{\rm Sm}] = \partial f_{\rm Sm}[T, n_{\rm Sm}]/\partial n_{\rm Sm}$ are the chemical potentials of the Hex-B and Sm-A phases, respectively, $f[T, n]$ is the free energy of the phase with density n (the number of molecules per unit volume for a fixed number of smectic layers), and indexes H and Sm correspond to the

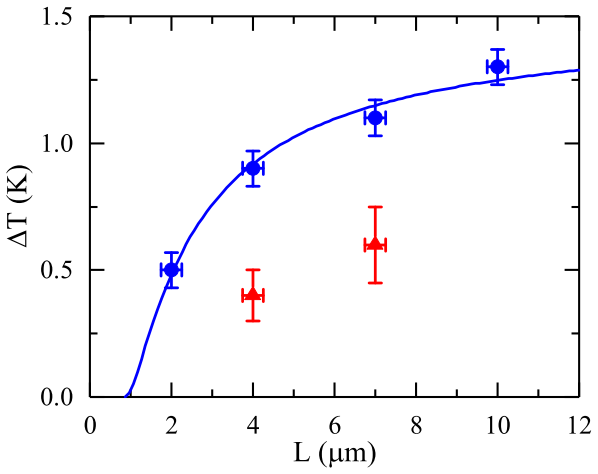

Figure 4. Temperature range ΔT of the Sm-A and Hex-B phase coexistence (two-phase region) as a function of the film thickness L. Blue circles correspond to data taken on cooling and red triangles - on heating of the 54COOBC films. Fitting of the data on cooling by Eq. (20) is shown by solid line.

Hex-B and Sm-A phases, respectively. The possibility of the finite temperature interval for the two phase coexistence suggests that neither of the phases can provide the correct density (only combination of both phases). This is similar to liquid-vapor coexistence in the pressuretemperature coordinates. We designate as $\varphi[T,n]$ the free energy density of the Sm-A phase per unit volume, $f_{\rm Sm}[T,n_{\rm Sm}]=\varphi[T,n_{\rm Sm}]$. In the vicinity of the TCP the free energy density $f_{\rm H}$ of the Hex-B phase (per unit volume) can be written according to conventional mean field theory [22, 43] as $f_{\rm H}[T,n_{\rm H}]=\varphi[T,n_{\rm H}]+g[\psi]$, where

$$g[\psi]=a|\psi|^2-\lambda|\psi|^4/6+\zeta|\psi|^6/90 \qquad (7)$$

is the Landau functional for the order parameter ψ (per unit area) and a, λ and ζ are Landau coefficients which depend on T and n. The coefficients a and λ are assumed to be small (they vanish at the TCP) and $\lambda>0$ for a first-order transition. We consider a relatively narrow temperature interval where the Hex-B and Sm-A phases coexist. Therefore the coefficient ζ remains approximately constant in this interval, whereas coefficient a has a standard form [22, 43] $a=\alpha\tau$, where $\alpha>0$ is a constant and $\tau=(T-T_0)/T_0$. The coefficient a vanishes at a certain temperature T_0 which is in the vicinity of TCP close to the temperature of the bulk Sm-A – Hex-B phase transition (where straightforward analysis of the Landau functional (7) yields to $a_c=5\lambda^2/8\zeta$, i.e. at $\tau_c=5\lambda^2/(8\alpha\zeta)$, $|\psi_c|^2=15\lambda/2\zeta$).

The order parameter ψ in the Hex-B phase is determined by minimization of expression (7):

$$|\psi_{\rm H}|^2=(5\lambda/\zeta)(1+\sqrt{1-6a\zeta(5\lambda^2)^{-1}})\ , \qquad (8)$$

which is real for $a<a_+$, where $a_+=5\lambda^2/6\zeta$. This gives a condition of existence of the Hex-B phase. In turn, assuming a small difference Δn between $n_{\rm Sm}$ and $n_{\rm H}$, $n_{\rm H}=n_{\rm Sm}-\Delta n$, and minimizing expression (7) with respect to the order parameter ψ, from Eq. (6) we obtain

$$\Delta n=\frac{\partial a}{\partial n}\left(\frac{\partial\mu}{\partial n}\right)^{-1}|\psi|^2\ , \qquad (9)$$

where $\mu=\partial\varphi/\partial n$ and where we discard high orders of $|\psi|^2$. Upon diminishing T the parameter a monotonically decreases and turns to zero ($a_{=}0$). At this point the smectic phase becomes absolutely unstable. Thus, from condition $a_-<a<a_+$ one can find that the equilibrium between Hex-B and Sm-A phases occurs in bulk in the interval

$$\Delta T=\frac{5\lambda^2}{6\alpha\zeta}\,T_0\ . \qquad (10)$$

To take surface effects into account, one should include the gradient term into the Landau functional for the field ψ (per unit area). Then we obtain for the free energy of the film

$$\mathcal{F}=S\int_{-L/2}^{L/2}dz\left\{b\,(\partial_z\psi)^2+g[\psi]\right\}\ , \qquad (11)$$

where $b>0$, z-axis is perpendicular to the film and $z=\pm L/2$ correspond to free surfaces of FSF of thickness L and surface area S. We assume in the following that the phase of the hexatic order parameter ψ is fixed, and therefore one can use real values of ψ. Due to the symmetry properties of FSF we have condition $\partial_z\psi[0]=0$ in the middle of the film. Minimization of Eq. (11) with respect to ψ gives Euler-Lagrange equation, which can be integrated once to yield

$$b(\partial_z\psi)^2=g[\psi]+C_1\ , \qquad (12)$$

where $C_1=-g[\psi_m]$, $\psi[z=0]\equiv\psi_m$. At $z\to 0$ the solution for $\psi[z]$ approaches its asymptotic bulk value, i.e. $\psi_m\approx\psi_{\rm H}$ in the Hex-B phase and $\psi_m\approx 0$ in the Sm-A phase. In above we have used the assumption $L\gg\xi_z$, which is true for the thick FSF under consideration. Here $\xi_z=\sqrt{b/(\alpha\tau)}$ is the hexatic correlation length along z axis, which is much larger than the molecular size close to the TCP.

There are two contributions to the free energy of the film $\mathcal{F}$: the bulk energy $\mathcal{F}^{(b)}=g[\psi_{\rm H}]\,LS$ and surface energy $\mathcal{F}^{(s)}$. The last one can be found after subtracting $\mathcal{F}^{(b)}$ from expression (11). With the use of Eq. (12) we can obtain

$$\mathcal{F}^{(s)}=2\,b\,S\int_{-L/2}^{L/2}dz\ (\partial_z\psi)^2\ . \qquad (13)$$

Assuming that $\psi^{(s)}\gg\psi_{\rm H}$ [44], where $\psi^{(s)}$ is the surface value of ψ, it follows from Eqs. (7) and (12) that in

both phases it exists a region near the surface where ψ^6 becomes a leading term on the right-hand side of Eq. (12), i.e. it can be written as

$$b(\partial_z\psi)^2 \,=\, \zeta\,\psi^6/90\;. \tag{14}$$

In this case the solution of Eq. (14) gives the following dependence for ψ^2 within a region near the surface (for $z>0$):

$$\psi^2 \approx \frac{(\psi^{(s)})^2}{1+(\psi^{(s)})^2\sqrt{2\zeta/(45b)}\,(L/2-z)} \qquad \left(\text{for } \frac{L}{2}-z \ll \frac{2\sqrt{2\,b\,\zeta}}{\sqrt{5}\,\lambda}\right), \tag{15}$$

which is valid for both phases. The surface value of ψ is denoted for the Hex-B and Sm-A phases as $\psi_{\rm H}^{(s)}$ and $\psi_{\rm Sm}^{(s)}$, respectively ($\psi_{\rm H}^{(s)} > \psi_{\rm Sm}^{(s)}$). These values should be substituted in Eq. (15) to obtain the corresponding z-dependencies of ψ^2 for each of the phases.

The analysis of solution of Eq. (12) indicates that even in the Sm-A phase the hexatic order diminishes from its surface magnitude to value $\sim \psi_{\rm H}/2$ within an extended range $\sim \xi_z\,\ln[\tau-\tau_c]$. This is a manifestation of an essential increase of the penetration length of hexatic ordering in FSF close to TCP.

Substituting the above solution into Eq. (13) one obtains main contributions to the surface energy. Using expressions (13) and (12) one finds the difference between the surface energies of the Hex-B and Sm-A phases

$$\frac{\Delta\mathcal{F}^{(s)}}{4\sqrt{b}S} = \int_{\psi_{\rm H}}^{\psi_{\rm H}^{(s)}} d\psi\sqrt{g[\psi]-g[\psi_{\rm H}]} - \int_0^{\psi_{\rm Sm}^{(s)}} d\psi\sqrt{g[\psi]}\,. \tag{16}$$

Using equation $\partial g[\psi_{\rm H}]/\partial\psi_{\rm H}=0$, we obtain from Eq. (16)

$$\Delta\mathcal{F}^{(s)} = (b\zeta)^{1/2} w[\psi_{\rm H}^2\zeta/\lambda]\,\psi_{\rm H}^4\,S\;, \tag{17}$$

where $w[\psi_{\rm H}^2\zeta/\lambda]$ is a dimensionless function that depends on the surface values of ψ. The exact values of ψ can be obtained only numerically ($\psi_{\rm H}^2\zeta/\lambda\sim 1$ - as it follows from Eq. (8)):

$$w[y_{\rm H}^2] \,=\, 4\sqrt{\frac{5}{3}}\left\{5\left(1+\sqrt{1-\frac{2}{5}\,y_{\rm H}^2\left(1-\frac{y_{\rm H}^2}{10}\right)}\right)\right\}^{-3/2} \times\left\{\int_{y_{\rm H}}^{y_{\rm H}^{(s)}} dy\sqrt{\widetilde{g}[y]-\widetilde{g}[y_{\rm H}]} - \int_0^{y_{\rm Sm}^{(s)}} d\psi\sqrt{\widetilde{g}[y]}\right\}, \tag{18}$$

where $y^2=\psi^2\zeta/\lambda$ ($y_{\rm H}^2=\psi_{\rm H}^2\zeta/\lambda$),

$$\widetilde{g}[y] \,=\, \left\{1-\frac{y_{\rm H}^2}{10}\right\}y^2 - \frac{y^4}{2\,y_{\rm H}^2} + \frac{y^6}{30\,y_{\rm H}^2}\;. \tag{19}$$

The typical dependence of the function $w[y_{\rm H}^2]$ on its argument containing several hexatic parameters is presented in Fig. 5.

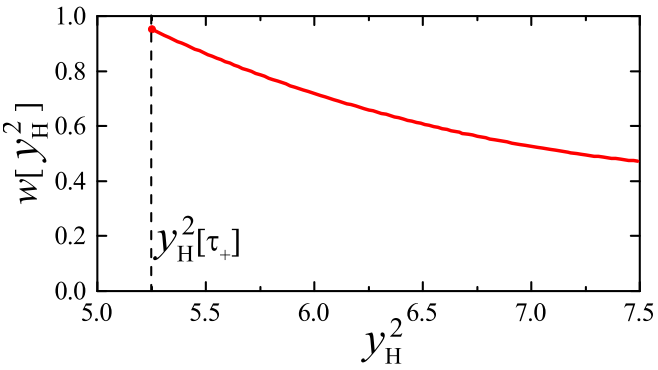

Figure 5. Dependence of the function $w[y_{\rm H}^2]$ on $y_{\rm H}^2$ for the typical values of material constants $\alpha=10^8$J m^{-3}, $\lambda=2\cdot 10^3$J m^{-3}, $\zeta=10^7$J m^{-3}, $b=10^{-14}$J m^{-1}. The simulations were performed for $\psi_{\rm H}^{(s)}=4.52\psi_{\rm H}$ and $\psi_{\rm Sm}^{(s)}=2.52\psi_{\rm H}$. The region of real values of $\psi_{\rm H}$ is located on the right side from the vertical dashed line, $\tau_+=a_+/\alpha$.

Comparing the difference between the surface energies of the Hex-B and Sm-A phases in Eq. (17) with the bulk energy $\mathcal{F}^{(b)}$ we conclude that surface effects produce an effective positive correction $\delta\lambda\simeq 6\,(b\zeta)^{1/2}\,w[\psi_{\rm H}^2\zeta/\lambda]\,L^{-1}$ to the coefficient λ. Using Eq. (10) we finally arrive to

$$\Delta T = \frac{5\lambda^2}{6\alpha\zeta}\,T_0\left(1-\frac{L_0}{L}\right)^2\;, \tag{20}$$

where

$$L_0 = \frac{6\,(b\zeta)^{1/2}}{\lambda}\,w[\psi_{\rm H}^2\zeta/\lambda] \tag{21}$$

is a characteristic length scale. Eq. (20) is valid for the film thickness $L\gg L_0$. Fitting of the experimental data with Eq. (20) shows a good agreement with theoretical predictions (see Fig. 4), and gives $L_0=0.9$ μm. As soon as the value of $w[\psi_{\rm H}^2\zeta/\lambda]$ is of the order of unity, it follows from Eq. (21) that the value of L_0 is determined by the hexatic correlation length along z axis (one can see from above that $\xi_z\sim\sqrt{b/(\alpha\tau_c)}\simeq\sqrt{b\,\zeta}/\lambda$, that is the main factor in Eq. (21)), which has to be much larger than the molecular length ($\sim 3\cdot 10^{-9}$ m) close to the TCP, i.e. more than by two orders of magnitude.

CONCLUSIONS

In conclusion, we report detailed spatially resolved x-ray studies of a first-order Sm-A–Hex-B phase transition in free standing films of 54COOBC of various thickness. Microfocused x-ray diffraction in combination with XCCA technique allowed us directly observe coexistence of the Sm-A and Hex-B phases. Experimentally measured temperature dependence of such structural parameters as C_6, ξ, and q_0 exhibits discontinuous behavior at the transition temperature, which was not observed for

the second-order Sm-A–Hex-B phase transition in other compounds [26]. We also found that the width of the two-phase coexistence region ΔT at the Sm-A–Hex-B transition becomes narrower for thinner films, reaching the value of about 500 mK for a 2 µm thick film. This indicates that the phase behavior of the 54COOBC films is strongly affected by the surface hexatic ordering field, which penetrates to interior layers of the film over large distances induced by the proximity of the Sm-A–Hex-B transition in 54COOBC to a TCP. An analytical expression for ΔT obtained from the Landau mean field theory is in a good agreement with the experimental data. This gives a unique possibility to approach TCP at the Sm-A–Hex-B phase transition line by varying the film thickness and experimentally investigate general properties of the phase transitions in the vicinity of the TCP. This new approach is quite general and can be applied to a large class of systems exhibiting TCPs, for example, helimagnetic films [45], or recently discovered materials with skyrmionic magnetic lattices [12, 13].

ACKNOWLEDGEMENTS

We acknowledge E. Weckert for fruitful discussions and support of the project, F. Westermeister for the support during the experiment, A. R. Muratov for theoretical discussions, and R. Gehrke for careful reading of the manuscript. The work of R. M. Khubbutdinov, E. S. Pikina and B. I. Ostrovskii was supported by the Russian Science Foundation (Grant No. 18-12-00108). N. A. Clark acknowledges support of U.S. National Science Foundation Grants DMR1420736 and DMR1710711. The work of V. V. Lebedev and E. I. Kats was supported by the Ministry of Science and Higher Education of Russia within the State assignment (theme No. 0033-2018-0003, Reg. No. AAAA-A18-118042790132-2). The work of I. A. Zaluzhnyy, R. P. Kurta, N. Mukharamova, Y. Y. Kim, and I. A. Vartanyants was supported by the Helmholtz Associations Initiative and Networking Fund and the Russian Science Foundation (project No. 18-41-06001).

* Corresponding author: elenapikina@itp.ac.ru
† Corresponding author: ostrenator@gmail.com
‡ Corresponding author: ivan.vartaniants@desy.de

[1] P. Chaikin and T. Lubensky, *Principles of Condensed Matter Physics* (Cambridge University Press, Cambridge, 1995).
[2] B. Fultz, *Phase Transitions in Materials* (Cambridge University Press, Cambridge, 2014).
[3] P. de Gennes and J. Prost, *The Physics of Liquid Crystals*, 2nd ed. (Oxford University Press, New York, 1993).
[4] P. Bolhuis and D. Frenkel, Phys. Rev. Lett. **72**, 2211 (1994).
[5] E. Słyk, W. Rżysko, and P. Bryk, J. Chem. Phys. **141**, 044910 (2014).
[6] Y. Lee, S. Jo, W. Lee, H. Lee, Y. S. Han, and D. Y. Ryu, Polymer **112**, 427 (2017).
[7] S. Mao, Q. MacPherson, and A. J. Spakowitz, Phys. Rev. Lett. **120**, 067802 (2018).
[8] J. Thoen, H. Marynissen, and W. Van Dael, Phys. Rev. Lett. **52**, 204 (1984).
[9] B. M. Ocko, R. J. Birgeneau, J. D. Litster, and M. E. Neubert, Phys. Rev. Lett. **52**, 208 (1984).
[10] M. A. Anisimov, P. E. Cladis, E. E. Gorodetskii, D. A. Huse, V. E. Podneks, V. G. Taratuta, W. van Saarloos, and V. P. Voronov, Phys. Rev. A **41**, 6749 (1990).
[11] A. Bauer, M. Garst, and C. Pfleiderer, Phys. Rev. Lett. **110**, 177207 (2013).
[12] M. Garst, J. Waizner, and D. Grundler, J. Phys. D **50**, 293002 (2017).
[13] J. Mulkers, K. M. D. Hals, J. Leliaert, M. V. Milošević, B. Van Waeyenberge, and K. Everschor-Sitte, Phys. Rev. B **98**, 064429 (2018).
[14] P. Oswald and P. Pieranski, *Smectic and Columnar Liquid Crystals* (Taylor & Francis Group, Boca Raton, 2006).
[15] W. H. de Jeu, B. I. Ostrovskii, and A. N. Shalaginov, Rev. Mod. Phys. **75**, 181 (2003).
[16] D. R. Nelson, *Defects and Geometry in Condensed Matter Physics* (Cambridge University Press, Cambrige, 2002).
[17] J. M. Kosterlitz, Rep. Prog. Phys. **79**, 026001 (2016).
[18] L. Agosta, A. Metere, and M. Dzugutov, Phys. Rev. E **97**, 052702 (2018).
[19] R. Pindak, D. E. Moncton, S. C. Davey, and J. W. Goodby, Phys. Rev. Lett. **46**, 1135 (1981).
[20] J. D. Brock, A. Aharony, R. J. Birgeneau, K. W. Evans-Lutterodt, J. D. Litster, P. M. Horn, G. B. Stephenson, and A. R. Tajbakhsh, Phys. Rev. Lett. **57**, 98 (1986).
[21] T. Stoebe and C. C. Huang, Int. J. Mod. Phys. B **9**, 2285 (1995).
[22] L. D. Landau and E. M. Lifshitz, *Course of Theoretical Physics, Statistical Physics, Part 1* (Pergamon Press, New York, 1980).
[23] A. J. Jin, M. Veum, T. Stoebe, C. F. Chou, J. T. Ho, S. W. Hui, V. Surendranath, and C. C. Huang, Phys. Rev. E **53**, 3639 (1996).
[24] H. Haga, Z. Kutnjak, G. S. Iannacchione, S. Qian, D. Finotello, and C. W. Garland, Phys. Rev. E **56**, 1808 (1997).
[25] R. P. Kurta, B. I. Ostrovskii, A. Singer, O. Y. Gorobtsov, A. Shabalin, D. Dzhigaev, O. M. Yefanov, A. V. Zozulya, M. Sprung, and I. A. Vartanyants, Phys. Rev. E **88**, 044501 (2013).
[26] I. A. Zaluzhnyy, R. P. Kurta, E. A. Sulyanova, O. Y. Gorobtsov, A. G. Shabalin, A. V. Zozulya, A. P. Menushenkov, M. Sprung, A. Krowczynski, E. Gorecka, B. I. Ostrovskii, and I. A. Vartanyants, Soft Matter **13**, 3240 (2017).
[27] B. Van Roie, K. Denolf, G. Pitsi, and J. Thoen, Eur. Phys. J. E **16**, 361 (2005).
[28] F. Mercuri, S. Paoloni, M. Marinelli, R. Pizzoferrato, and U. Zammit, J. Chem. Phys. **138**, 074903 (2013).
[29] A. J. Jin, M. Veum, T. Stoebe, C. F. Chou, J. T. Ho, S. W. Hui, V. Surendranath, and C. C. Huang, Phys. Rev. Lett. **74**, 4863 (1995).
[30] C.-F. Chou, J. T. Ho, S. W. Hui, and V. Surendranath, Phys. Rev. Lett. **76**, 4556 (1996).

[31] C.-F. Chou, A. J. Jin, S. W. Hui, C. C. Huang, and J. T. Ho, Science **280**, 1424 (1998).
[32] V. Surendranath, D. L. Fishel, A. de Vries, R. Mahmood, and D. L. Johnson, Mol. Cryst. Liq. Cryst. **131**, 1 (1985).
[33] I. A. Zaluzhnyy, R. P. Kurta, E. A. Sulyanova, O. Y. Gorobtsov, A. G. Shabalin, A. V. Zozulya, A. P. Menushenkov, M. Sprung, B. I. Ostrovskii, and I. A. Vartanyants, Phys. Rev. E **91**, 042506 (2015).
[34] P. Wochner, C. Gutt, T. Autenrieth, T. Demmer, V. Bugaev, A. D. Ortiz, A. Duri, F. Zontone, G. Grübel, and H. Dosch, Proc. Natl. Acad. Sci. USA **106**, 11511 (2009).
[35] M. Altarelli, R. P. Kurta, and I. A. Vartanyants, Phys. Rev. B **82**, 104207 (2010), Erratum: Phys. Rev. B **86**, 179904 (2012).
[36] R. P. Kurta, M. Altarelli, and I. A. Vartanyants, Adv. Condens. Matter Phys. **2013**, 959835 (2013).
[37] R. P. Kurta, M. Altarelli, and I. A. Vartanyants, "Structural analysis by x-ray intensity angular cross correlations," in *Adv. Chem. Phys.*, Vol. 161 (John Wiley & Sons, Inc., 2016) Chap. 1, pp. 1–39.
[38] J. Brock, D. Noh, B. McClain, J. Litster, R. Birgeneau, A. Aharony, P. Horn, and J. Liang, Z. Phys. B - Condensed Matter **74**, 197 (1989).
[39] T. Stoebe, R. Geer, C. C. Huang, and J. W. Goodby, Phys. Rev. Lett. **69**, 2090 (1992).
[40] I. A. Zaluzhnyy, R. P. Kurta, A. P. Menushenkov, B. I. Ostrovskii, and I. A. Vartanyants, Phys. Rev. E **94**, 030701 (2016).
[41] G. Aeppli and R. Bruinsma, Phys. Rev. Lett. **53**, 2133 (1984).
[42] S. C. Davey, J. Budai, J. W. Goodby, R. Pindak, and D. E. Moncton, Phys. Rev. Lett. **53**, 2129 (1984).
[43] A. Z. Patashinskii and V. L. Pokrovskii, *Fluctuation Theory of Phase Transitions* (Pergamon Press, Oxford, 1979).
[44] The bulk value of the hexatic order parameter in the Sm-A phase is zero, and near the TCP it is small in the Hex-B phase. However, experimental data in Sm-A FSFs [**? ? ? ?**] suggest that the surface value of the hexatic order parameter is much larger than its bulk value. Simulations performed in this work were made under this assumption.
[45] M. Janoschek, M. Garst, A. Bauer, P. Krautscheid, R. Georgii, P. Böni, and C. Pfleiderer, Phys. Rev. B **87**, 134407 (2013).